

# The effect of paleo-oceanographic changes on the sedimentary recording of hydrothermal activity in the Red Sea during the last 30,000 years

Aoua Sougo Coulibaly<sup>a,1</sup>, Pierre Anschutz<sup>a,\*</sup>, Gérard Blanc<sup>a</sup>, Bruno Malaize<sup>a</sup>,  
Claude Pujol<sup>a</sup>, Christophe Fontanier<sup>a,b,c</sup>

<sup>a</sup> UMR Environnements et Paléo-environnements OCéaniques (EPOC), Université Bordeaux 1, 33405 Talence, France

<sup>b</sup> Laboratory for the Study of Recent and Fossil Bio-Indicators, Angers University, UPRES EA 2644,  
2 Boulevard Lavoisier, 49045 Angers Cedex, France

<sup>c</sup> Laboratory for the Study of Marine Bio-indicators (LEBIM), 85350 Ile d'Yeu, France

Received 12 October 2004; received in revised form 30 August 2005; accepted 18 September 2005

## Abstract

The restricted exchange of water with the Indian Ocean makes the Red Sea extremely sensitive to global oceanographic changes, such as sea-level variations linked with Quaternary climate change. The 120 m global sea level lowering during the last glacial maximum caused great reduction in water exchange with the open ocean. At that time, salinities reached 50‰, and were beyond the tolerance of planktonic foraminifera. Some topographic depressions located on the Red Sea axial zone are the centre of hydrothermal activity. They are filled with hot brines and contain metalliferous sediments. We studied three sediment cores in the axial part of the Red Sea, one from the metal-rich Suakin Deep depression, and two cores sampled outside any deep, at two different depths. The sediment of the core located in the anoxic brine-filled Suakin Deep contained no benthic foraminifera, indicating the deep was filled by a brine pool during the recovered period of marine isotopic stages 1, 2, and 3. The distribution of benthic foraminifera in the two other cores indicates that Red Sea waters were saltier during stage 2 and 3 than today, and that at 2000 m depth, Red Sea waters were anoxic during stage 2 and dysoxic during stage 3. Profiles of Fe, Mn, and Zn indicate that the sedimentary flux of metals was higher during stage 1 than during stage 2 in hydrothermal brine-filled deeps. In contrast, the sedimentary flux of metal in cores outside the anoxic depressions was higher during stage 2. The shape of the metal profiles can be attributed to hydrological changes that induced variations of redox conditions in water column during isotopic stage 1, 2, and 3. During interglacial periods, metals dissolved in anoxic brines precipitated at the redox boundary that corresponded to the brine–seawater interface, so that metals precipitated only in the deeps. During glacial period, the deep water was anoxic, and the redox boundary was located above the brine–seawater interface. Therefore, the hydrothermal metals could diffuse into the anoxic deep Red Sea water and be precipitated over a large area. This interpretation suggests that the observed variations of metal concentrations are not only related to fluctuations of the hydrothermal fluid discharge, but also to the varying redox conditions in the deep Red Sea water.

© 2005 Elsevier B.V. All rights reserved.

**Keywords:** Red Sea; hydrothermal; paleo-oceanography; proxy; Quaternary; geochemistry; sediment

\* Corresponding author. Tel.: +33 540 008 873; fax: +33 556 840 848.

E-mail address: p.anschutz@epoc.u-bordeaux1.fr (P. Anschutz).

<sup>1</sup> Present address: Department of Earth Sciences, University Cocody, Abidjan, Ivory Coast.

## 1. Introduction

Water exchange between the Red Sea and the open ocean takes place across the shallow sill of Bab El Mandeb (105 km wide, maximum depth 137 m; Werner and Lange, 1975), and through a narrow channel close to Perim Island (20 km wide, 300 m depth; Morcos, 1970). Negligible land drainage and precipitation with respect to a very high evaporation rates of  $208 \text{ cm yr}^{-1}$  (Ahmad and Sultan, 1987) over the entire Red Sea, results in a convective anti-estuarine basin circulation, with surface water inflow compensated by a subsurface outflow across the sill. The restricted nature of the Red Sea basin makes it extremely sensitive to global oceanographic changes, such as Quaternary climate and associated sea-level variations (Siddall et al., 2003).

It is known that during Quaternary, climate underwent strong fluctuations from glacial to interglacial periods. The 120 m global sea level lowering during the last glacial maximum (Fairbanks, 1989) caused great changes within the Red Sea basin through a great reduction in water exchange with the open ocean across the shallow and narrow sill. Reduction of exchange with the Indian Ocean caused a salinity crisis in the Red Sea during the last glaciation (Locke and Thunell, 1987; Thunell et al., 1988). Salinities reached 50‰, and were beyond the tolerance of planktonic foraminifera, so that an aplanktonic zone developed (Deuser et al., 1976; Ivanova, 1985; Locke and Thunell, 1987; Thunell et al., 1988; Almogi-Labin et al., 1991; Hemleben et al., 1996; Fenton et al., 2000).

One of the main characteristics of the Red Sea is the numerous topographic depressions located in the axial zone (Miller et al., 1966). These depressions are the centre of hydrothermal activity. They are filled with brines and/or contained metalliferous sediments (Bäcker et al., 1975; Zierenberg and Shanks, 1988; Blanc and Anschutz, 1995; Scholten et al., 2000). Atlantis II Deep is the largest brine-filled basin of the Red Sea ( $60 \text{ km}^2$ ). It is also the most studied among all the Red Sea deeps. Different sedimentary units have been defined for the basin (Bäcker et al., 1975; Anschutz and Blanc, 1995). The bottom of the sequence consists of biogenic and detrital sediments enriched in metalliferous particles, deposited on a basaltic substratum during the marine isotopic stage (MIS) 2 (Ku et al., 1969; Shanks III and Bischoff, 1980; Anschutz and Blanc, 1995). The overlying metalliferous sediment consists of sulphide and Fe- and Mn-oxide bearing facies. From these lithostratigraphic descriptions it appears that metalliferous fraction is dominant in the Holocene deposits (MIS 1), and minor below (MIS 2). This repartition has been attrib-

uted to the intensification of hydrothermal activity during isotopic stage 1 (Anschutz and Blanc, 1995).

Little stratigraphic data exist from other metal-enriched deeps of the Red Sea, to allow any correlation between climatic fluctuations, sea-level changes, and hydrothermal activity. The specific objective of this study was to determine the main factors responsible for the timing of hydrothermal activity, and its sedimentary record in the Red Sea. This study was based on the geochemical and stratigraphic description of three sediment cores collected at different sites, one in a metal-rich depression, and two cores sampled outside any deep, at two different depths. We use the distribution of solid Fe, Mn, and Zn as proxies of hydrothermal particles in the sediment. The stratigraphy of the cores was determined using radiocarbon dating, foraminifera distribution, stable isotopic stratigraphy, and the position of reference facies of Red Sea sediments.

## 2. Sampling and methods

### 2.1. Sampling

The cores were collected with the RV *Marion Dufresne*, during Leg 73, in September 1992 (Fig. 1). Core MD92-1034 ( $21^{\circ}20.55'N$ ,  $37^{\circ}57.09'E$ ; 7.95 m

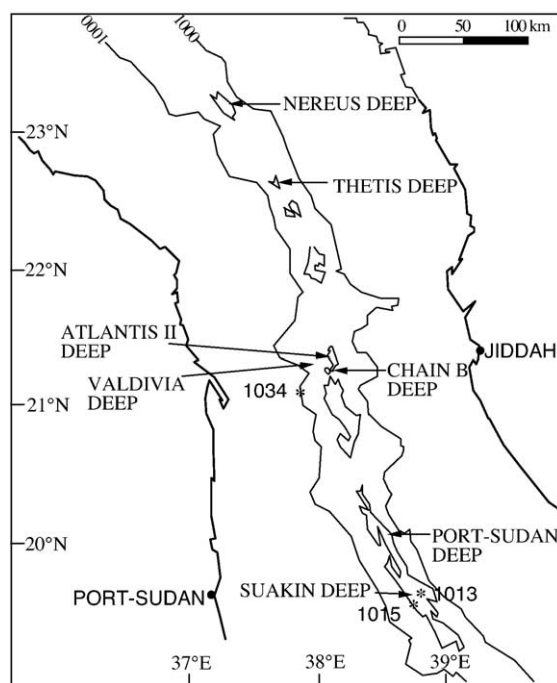


Fig. 1. Map of the central Red Sea showing the isobath 1000 and 2000 m, and the position of the cores 1013, 1015, and 1034, collected during the cruise MD73.

long) was sampled outside the axial zone, core MD92-1013 (19°36.49'N, 38°43.64'E; 5.8 m long) in the Suakin Deep, and core MD92-1015 was sampled nearby, but outside the deep, in the Suakin Plain (19°37.55'N, 38°37.71'E; 15.8 m long).

The core 1034 was taken at a water depth of 990 m (Fig. 1). Sediments consist of a beige-to-grey homogeneous pelagic carbonate ooze. The core also contains a coarse zone with abundant carbonate crusts near the top (Fig. 2). Carbonate crusts are well known in Red Sea sediments. They have been studied in detail by Milliman et al. (1969), and correspond to the glacial isotope stage 2 (12–24 ky BP). They are overlaid by an olive grey layer enriched in organic carbon. The core 1013 was collected in Suakin Deep at 2800 m depth. The Suakin depression is filled by a brine pool from 2770 m to the bottom (Baumann et al., 1973; Anschutz et al., 1999). The core 1013 was collected in the western basin. The sediment consists of layered muds dominated by detrital silicates and biogenic carbonates, and contains metallif-

erous particles (Pierret et al., 2000). The core also contains two dark horizons enriched in organic matter, and a thick carbonate crust layer at the bottom (Fig. 2). The core 1015 was taken at a water depth of 1969 m in the Suakin plain. The Suakin plain is located in the Red Sea axial zone, close to the Suakin Deep. The core 1015 was collected 10 km away from the Suakin Deep brine, and 700 m above the top of the present-day brine pool, i.e., far from the direct influence of the brine pool. The core includes four dark-grey horizons enriched in organic matter, and several turbidite layers (Fig. 2). No significant change in mineralogy have been noticed along the core (Hofmann et al., 1998).

A total of 366 samples of 1 cm thick were taken from these three cores, with a 5 cm sampling step. When the sediment colour and texture were homogeneous (example core 1034), a 10 cm sampling step was chosen. Two aliquots were extracted from each sample, to define foraminiferal and chemical variability along the sedimentary sequences.

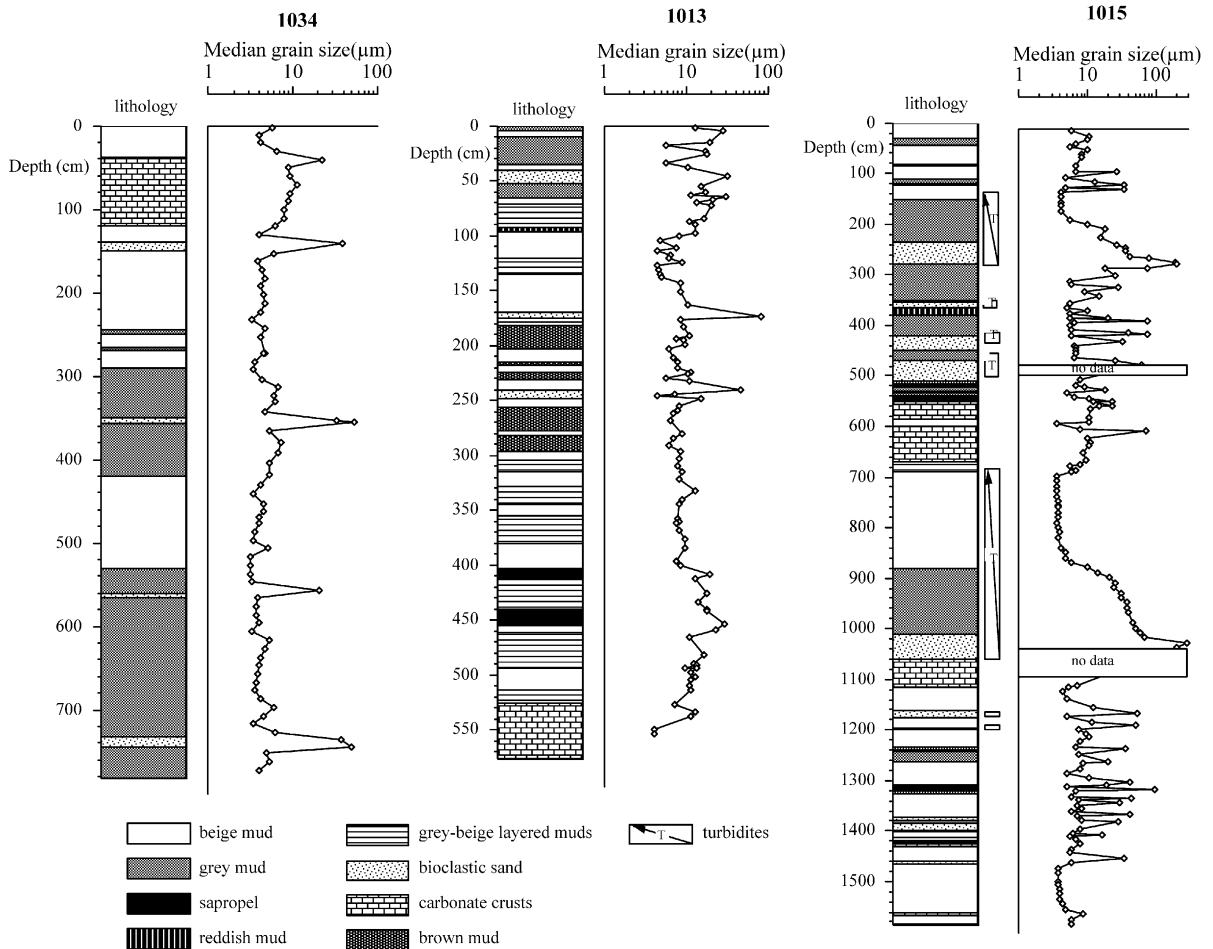


Fig. 2. Petrographic log and the profiles vs. depth of median grain size of the cores 1013, 1015, and 1034.

## 2.2. Methods

The grain size distribution was determined by using a laser diffractometer Malvern Mastersizer. The samples for micropaleontological analyses were thoroughly washed on 150 and 63  $\mu\text{m}$  mesh sieves. The sieved residues were dried at 70 °C during 24 h and weighted (to obtain the dry weight per sieve fraction). Qualitative and quantitative analyses of microfossils were performed on the 150  $\mu\text{m}$  fraction. The samples showing abundant microfauna were divided into aliquots containing approximately 300 planktonic foraminifera using a statistically correct micro-splitter. Various taxa were then counted and considered as a percentage of total fauna (relative abundance). The same fraction was also used for the qualitative study of benthic fauna.

Stable oxygen isotope analyses were made on *Globigerinoides ruber* picked up within the 250–350  $\mu\text{m}$  grain size fraction. The preparation of each aliquot (10 specimens), representing a mean weight of 80  $\mu\text{g}$ , was done using a Micromass Multiprep autosampler. The use of single species records avoided the vital effect fractionations. Stable isotope data were referred to the PDB standard notation and calibrated via NBS 19. Analytical precision of the carbonate standard was  $\pm 0.09\text{‰}$  and  $\pm 0.05\text{‰}$  for  $\delta^{18}\text{O}$  and  $\delta^{13}\text{C}$ , respectively.

Six AMS  $^{14}\text{C}$  dates were performed on the three cores; two on the core 1034, three on 1013, and one on 1015. Three other radiocarbon data for the core 1015 were taken from Hofmann et al. (1998). Preparation for AMS  $^{14}\text{C}$  dating involved picking of 150–250 mg of planktonic foraminiferal specimens in the samples. They were cleaned in a ultrasonic bath to avoid contamination by the fine sediment fraction. All the data are reported in radiocarbon years.

The samples for chemical analysis were freeze-dried for 24 h and grounded in an agate pestle and mortar. Chemical analysis of dried and powdered marine sediments is complicated by the presence of salt that precipitated during drying of the interstitial seawater or brine. Therefore, we measured the salt mass of each sediment sample of the core 1013 to correct for the mass used in the chemical analysis. For the determination of salt content, we added 1 ml of distilled water to 200 mg of powdered dried sediment. The mixture was vigorously shaken to dissolve the salt. After centrifuging at 3000 rpm for 1 min, the salt content was measured on 200  $\mu\text{l}$  of the supernatant using a refractometer.

For the analysis of Fe, Mn and Zn, a 50 mg sample of the powdered, dried sediment was digested during 48

h at 80 °C with 2 ml of 65%  $\text{HNO}_3$  in a prewashed polypropylene vial. Leaching of sediment with  $\text{HNO}_3$  does not yield a complete digestion of particles. However, the goal of the geochemical analyses was not to determine the whole-rock metal content, but it was to determine the evolution with time of hydrothermal metal input to the sediment.  $\text{HNO}_3$  extracts metals from sulphide, oxides, and carbonate minerals, which are the major metal-bearing phases in the Red Sea hydrothermal sediments (Pottorf and Barnes, 1983; Anschutz and Blanc, 1995). 100  $\mu\text{l}$  of the residual solution was evaporated on a hotplate and the dry residue was dissolved in 9.9 ml of 0.2 N HCl. Fe, Mn and Zn were analyzed by flame atomic absorption spectrometry (Perkin Elmer AA 300). The precision of the analyses, as determined from replicates, was better than 2%.

Particulate sulphur and carbon were quantified by infrared absorption photometry using a LECO CS-125. The carbonate content was measured in the whole samples with an automated calcimeter, which measured the volume of  $\text{CO}_2$  released by the dissolution of carbonates with HCl. The organic carbon fraction of the samples was determined by subtracting the amount of calcium carbonate from the total carbon content measured with the LECO CS-125. We obtained accurate concentrations of organic-C for the samples located in the sapropel horizons, where the  $\text{CaCO}_3$  content was lower (about 30%), and organic-C was high. Total S has been corrected for the pore water sulphate-S contribution; the latter has been determined from the salt content of dry samples, and the  $\text{SO}_4/\text{Cl}$  ratio of pore waters.

## 3. Results

### 3.1. Stratigraphy

Time-stratigraphic frameworks have been obtained for the cores studied through comparison between the oxygen isotope stratigraphy and the orbitally tuned ice volume model (SPECMAP, Imbrie et al., 1984). The core 1034 shows two sediment layers with a  $\delta^{18}\text{O}$  of *G. ruber* above +2‰, which can be attributed to the cold MIS 2 and 4 (Fig. 3). Two AMS  $^{14}\text{C}$  dating of the samples located above and below the upper layer with positive  $\delta^{18}\text{O}$  values confirm the stratigraphy. The sediment attributed to MIS 2 also contains carbonate crusts, which is typical of this period in the Red Sea. A dark grey layer enriched in organic carbon is present at 40 cm depth. This layer can be qualified as sapropelic horizon. A sapropelic horizon attributed to the boun-

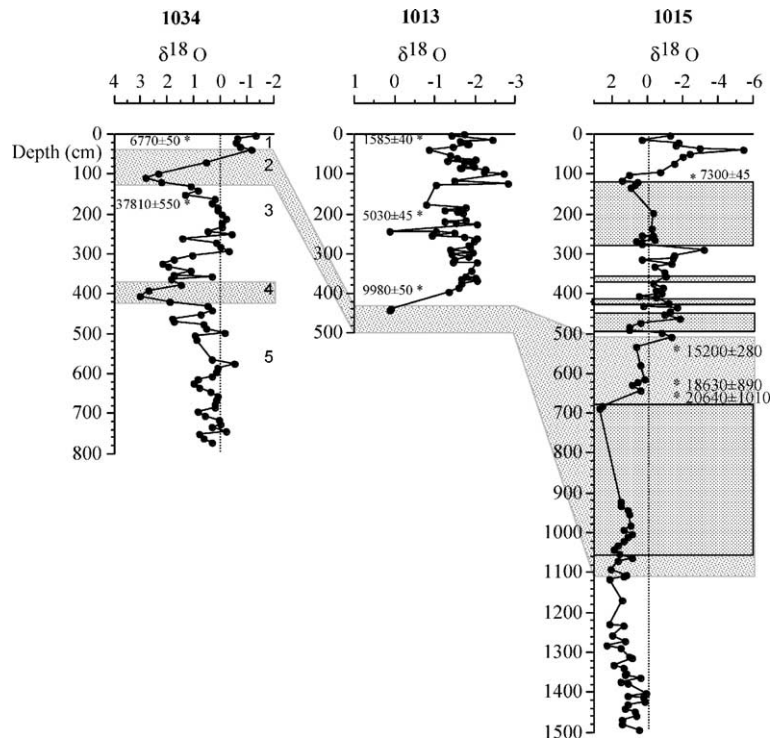


Fig. 3. Profiles vs. depth of stable oxygen isotope measured on *G. ruber*, in ‰ normalized vs. PDB standard. Numbers 1 to 5 at the right of core 1034 profile correspond to the marine isotopic stages. Ages indicated with (\*) are  $^{14}\text{C}$  AMS ages. The three ages in MIS 2 of the core 1015 are from Hofmann et al. (1998).

dary between MIS 1 and MIS 2 has been described in several sedimentary cores of the Red Sea (Ivanova, 1985). The isotopic and petrographic data indicate, therefore, that MIS 2 is recorded between 40 and 130 cm, and MIS 4 between 379 and 418 cm depth. The lithologic properties that define the limit between MIS 1 and MIS 2 (sapropel and carbonate crusts) are present at the bottom of the core 1013, below 4 m depth. An AMS  $^{14}\text{C}$  dating at 3.84 m depth gives an age of 9980 years. The oxygen isotopic composition of *G. ruber* remains negative in the upper core, which confirms that the top 4 m corresponds to MIS 1 (Fig. 3). The limit between the MIS 1 and MIS 2 occurs just below the first sapropelic horizon at 410 cm, and above the top of the carbonate crust located at 530 cm. The AMS  $^{14}\text{C}$  dating obtained in the core 1015 is in agreement with the dating obtained by Hofmann et al. (1998) on carbonate crusts of the same core. The sediment is enriched in sapropelic horizons between 518 and 550 cm depth, which suggests that the boundary between MIS 1 and MIS 2 occurs within this interval. The carbonate crusts of MIS 2 begin at 550 cm depth. The bottom of MIS 2 occurs at 1115 cm depth. The sediment of MIS 1 and 2 are interrupted by turbiditic deposits. The limits of the turbiditic layers have been

determined from the macroscopic description of the core, and from the distribution of grain size. The vertical profile of the median grain size of the core 1015 (Fig. 2) indicates that the turbiditic layers begin at the bottom with a median grain size above  $70\ \mu\text{m}$ , and stop with a fine-grained layer, with a median grain-size lower than  $5\ \mu\text{m}$ . A 380 cm thick turbidite takes place in the MIS 2 sediments, between 680 and 1060 cm depth. Turbidites are present in MIS 1, between 500 and 450 cm, 430 and 415 cm, 375 and 355 cm, and a large one between 280 and 135 cm.

The sedimentation rate is estimated from the AMS  $^{14}\text{C}$  dating, and the position of the main isotopic stages in the cores. Before interpolating, we have subtracted all the thicknesses of the turbidite layers from the core 1015 length, thus assuming that these layers were deposited instantaneously.

The sedimentation rate in the core 1034 varies between 3 and  $9\ \text{cm ky}^{-1}$ , which is in concordance with the values of  $3\text{--}10\ \text{cm ky}^{-1}$ , calculated in other cores of the Red Sea by Ivanova (1985). In the Suakin Deep (core 1013), the sedimentation rate is higher in the Holocene, with  $47\ \text{cm ky}^{-1}$ . High sedimentation rates probably result from a focussing of particles along the slopes of the Red Sea axis toward the Suakin depres-

sion. Very high sedimentation rates were also noticed in other depressions of the Red Sea, as for instance in the Atlantis II Deep, where values higher than  $1 \text{ m ky}^{-1}$  were calculated for the Holocene (Anschutz and Blanc, 1995). In the Suakin plain (core 1015), different sedimentation rates have been calculated. Omitting the turbiditic layers, little variation of sedimentation rate occurs along the core. It is  $16 \text{ cm ky}^{-1}$  in the carbonate crust of MIS 2, and  $20 \text{ cm ky}^{-1}$  in the sediment of MIS 1. Baumann et al. (1973) reported sedimentation rates of  $35\text{--}40 \text{ cm ky}^{-1}$  in the Suakin plain, which is close to the mean sedimentation rate of core 1015, when the turbiditic layers are included in the sediment column.

### 3.2. Fauna results

The studied cores contain mainly tropical-subtropical spinose species. *Globigerinoides ruber* is the most common species found in the sediment. It is accompanied by high abundances of *G. sacculifer*, *Hastigerina pelagica*, *G. rubescens*, *O. universa*, and *G. siphonifera* assembled into one entity, named the SPRUDTS group (Rohling et al., 1998). The vertical profile of total planktonic foraminifera per gram of sediment shows obvious dominance of full glacial influences on these records, marked by an aplanktonic zones with no or very few planktonic foraminifera in the autochthonous sediments (Fig. 4). This aplanktonic zone correlates with the glacial isotope stage 2 in all cores (Fenton et al., 2000).

The quantitative distribution of planktonic foraminifera (*G. ruber* and *G. sacculifer*) from MIS 4 to MIS 1 shows a succession of microfaunal assemblages characterising surface water changes. The core 1013 (Suakin Deep), shows the presence of three zones close to what is known from Berggren and Boersma (1969). Ecozone 1a above 175 cm depth, and ecozone 1c below 300 cm depth are characterised by the dominance of *G. sacculifer* (% *G. sacculifer* > % *G. ruber*). In ecozone 1b, between 175 and 300 cm depth, the percentage of the two species is equivalent (% *G. sacculifer* ~ % *G. ruber*). Ecozone 2 defined in MIS 2 is similar to that of Ivanova (1985), and is characterized by the absence of planktonic foraminifera. MIS 3 and 4 in core 1034 show the dominance of *G. ruber*.

The sediment of the core 1013 located in the anoxic brine-filled Suakin Deep contains no benthic foraminifera. A pilot study was carried out on the benthic foraminiferal content of the other cores, revealing only a few number of specimens over the different stage recorded. A meticulous study on the core 1015 (Suakin plain), revealed that the aplanktonic zone of MIS 2 was

characterized by absence of benthic foraminiferal species. *Bolivina* spp. are abundant in the sediment deposited during MIS 3, with *B. subreticulata* being the dominant species. The MIS 1 sediment above the aplanktonic zone is dominated by *Uvigerina* spp., mainly *Uvigerina hollicki*. *Cibicides ungerianus* is also present in abundance. These species characterize the interglacial periods in the Red Sea (Fenton et al., 2000). The dominant benthic foraminifera assemblage, which has been determined in MIS 1 and 3 of the core 1015, was also recognized in the core 1034, and also in the core MD92-1017, located at 570 m depth, and studied in details by Fenton et al. (2000). The sediment of stage 2 in the core 1034 (and 1017) shows a loss of diversity in the benthic foraminiferal faunas with an increased importance of the miliolid taxa (Table 1).

Monospecific assemblages of pteropod tests of the salinity tolerant epipelagic species *Creseis acicula* are noticed throughout the aplanktonic zones in the sediment cores, in agreement with the results of Almogi-Labin et al. (1986, 1991, 1998).

### 3.3. Geochemistry

The profiles of metals extracted with  $\text{HNO}_3$ , particulate sulphur, and inorganic carbon are plotted in Fig. 5. In the core 1034,  $\text{CaCO}_3$  deduced from the inorganic carbon represents between 60% and 80% of the whole rock. Fe, Mn, and Zn occur at low concentrations, in comparison with the other cores, with average concentrations of  $6.5$ ,  $0.6$ , and  $0.04 \text{ g kg}^{-1}$ , respectively (Table 2). They follow similar trend throughout the different isotopic stages recorded, with low variations. Maximum concentrations of Fe, Zn, and S, which are about three times the average values, are found in the sapropelic layer located just above the carbonate crust. This layer contains the lowest content of the core in calcium carbonate (39%), and the organic carbon concentration reaches 1.92 wt.%.

The sediment of Suakin Deep (core 1013) contains less carbonates than the sediment of the core 1034. Most of the sample concentrations are between 30% and 60%. Lower concentrations are found between 400 and 500 cm depth, at the top of MIS 2. This level also contains the highest sulphur concentrations (up to 12%). The carbonate content is lower than in the core 1034, probably because the carbonate particles are mixed with metalliferous particles. The core 1013 reveals variable, but high concentrations of Fe (17 to  $343 \text{ g/kg}$ ), Mn (0.8 to  $150 \text{ g/kg}$ ), and Zn (0.09 to  $2.16 \text{ g/kg}$ ). Iron and manganese-bearing minerals are hematite, ferrihydrite, manganite, and Mn-siderite (Pierret et al.,

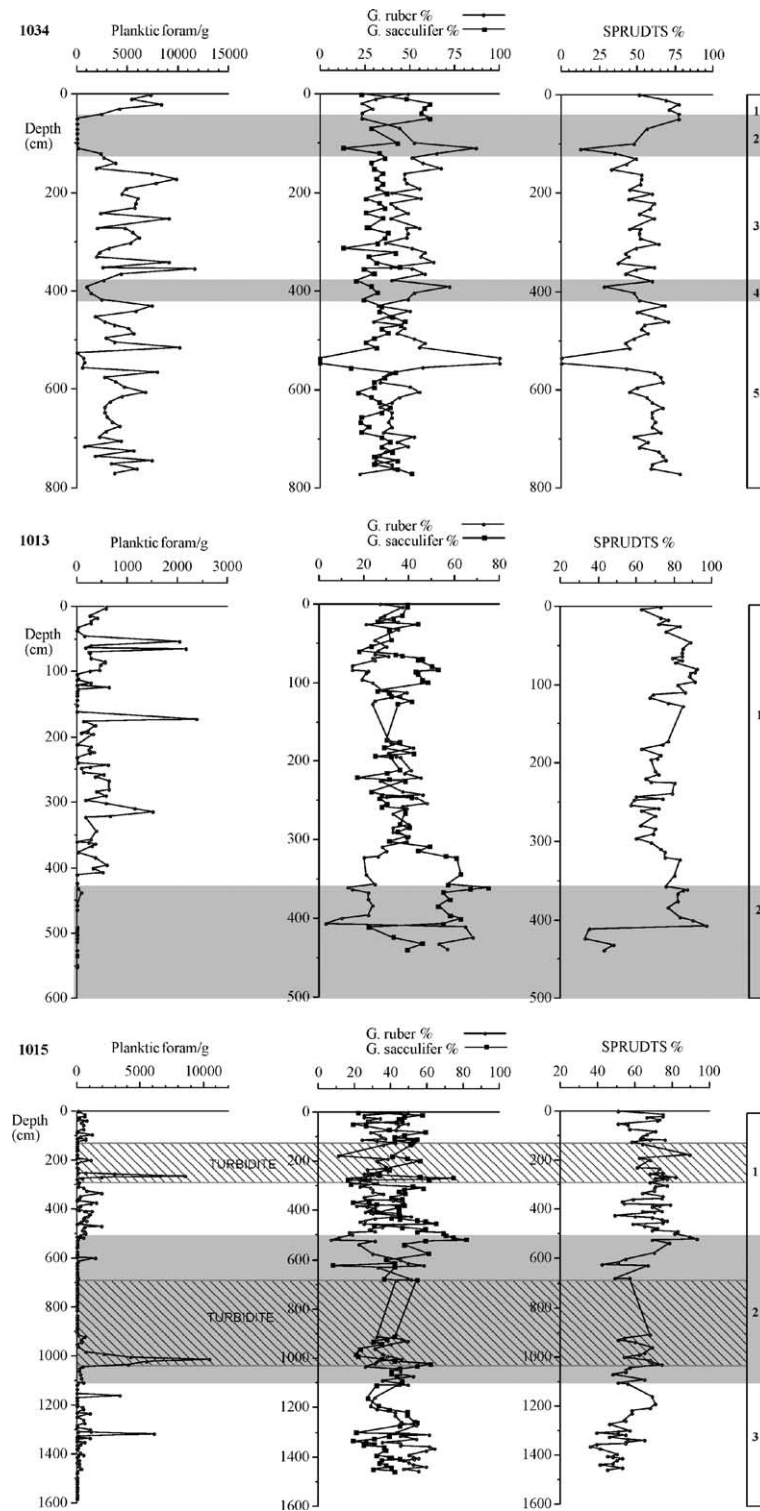


Fig. 4. Vertical profiles of abundance of planktonic foraminifera (left), relative abundance of *G. ruber* (line) and *G. sacculifer* (dots) (middle), and the proportion of SPRUDTS group (right).

Table 1

Summary of the distribution of dominant benthic foraminifera in cores 1034, 1015, and 1013

Core number	Water depth (m)	MIS 1	MIS 2	MIS 3
1034	1000	<i>Uvigerina hollicki</i> , <i>Cibicides ungerianus</i>	Miliolid taxa	<i>Bolivina subreticulata</i>
1015	2000	<i>Uvigerina hollicki</i> , <i>Cibicides ungerianus</i>	/	
1013	2800 (Suakin Deep)	/	/	/

2000). A clear-cut decrease of the Mn concentrations marks the boundary between MIS 1 and 2, with the lowest values in MIS 2. This trend occurs for the Zn concentrations, but it is less pronounced (Table 2).

The sediment taken from Suakin plain (core 1015) reveals intermediate concentrations. Most of the CaCO<sub>3</sub> concentrations are between 40% and 65%. Lower values are found between 500 and 550 cm depth, at the top of MIS 2, as in the other cores. This layer is also enriched in particulate sulphur. The mean metal concentrations in MIS 1 are about three times the concentrations in the core 1034. The particulate metal concentration of the MIS 2 sediments clearly shows the presence of the turbiditic layer between 680 and 1060 cm. The concentrations of Fe, Mn, and Zn decrease linearly from the fine-grained sediment of the top of the turbidite to the coarse-grained sediment of the bottom. This distribution is most likely due to the fact that metal-bearing particles belong to the fine-grained fraction. It is probably not a diagenetic effect, as described in deep sea turbidites (Buckley and Cranston, 1988), because the content of organic matter, that triggers diagenetic reactions and metal remobilization, is very low in the turbiditic layer of the core 1015. Above the turbiditic layer, the autochthonous sediment of MIS 2 presents a high variability of metal concentration. Some layers show metal concentrations which are high in comparison with the concentration measured in the sediment of MIS 1. The difference between MIS 1 and MIS 2 is the highest for the Mn concentrations (Table 2). The sediment of MIS 3 also reveals layers with high concentrations of metalliferous particles relative to those of MIS 1.

## 4. Discussion

### 4.1. Paleo-environment

Large variations are observed in the distribution of planktonic foraminifers, which are related to changes in sea surface salinities (Locke and Thunell, 1987; Thunell et al., 1988). Elevated salinities during the last glacial maximum (LGM) is held responsible for the aplanktonic zone, and the mono-specific assemblage of pteropods, found in sediments throughout the Red

Sea (Fenton et al., 2000). Surface water conditions approached or exceeded the tolerance limits of planktonic foraminifera (Ivanova, 1985; Locke and Thunell, 1987; Thunell et al., 1988; Almogi-Labin et al., 1991; Hemleben et al., 1996). The 120 m global glacio-eustatic sea level lowering during the LGM (Fairbanks, 1989) limited considerably water exchanges between the Red Sea and the Indian ocean, and caused a great increase of salinity in the Red Sea. The aplanktonic conditions corresponded to surface salinity  $\geq 49$ , and reached the studied zone (south-central Red Sea) from 22 ky BP (Fenton et al., 2000).

The absence of benthic foraminifera in the core 1013 suggests that anoxic brines were present in the Suakin Deep, at 2800 m depth, during MIS 2, and during the whole Holocene period, as proposed by Anschutz et al. (1999) from a brine residence time calculation. The absence of benthic foraminifera in the core 1015 during MIS 2 suggests that the bottom waters of the Red Sea were also anoxic during this period at 2000 m depth. At the same period, the bottom waters located at 1000 m depth (core 1034) or above (e.g. core 1017, Fenton et al., 2000, or the cores studied by Hemleben et al., 1996) were probably not anoxic, because the sediment contains benthic foraminifera, dominated by miliolid taxa, which are known from hypersaline marine environments around the Red Sea (Halicz and Reiss, 1981). Therefore, an oxycline, which was probably associated with a halocline, occurred during MIS 2 in the Red Sea deep waters, between 1000 and 2000 m depth. To our knowledge, no core has been studied for micropaleontological purpose within this depth interval in that part of the Red Sea. New cores should be collected on a depth transect below 1000 m to precise the extent of the anoxia during the LGM.

*Cibicides* spp. and *Bolivina* spp. are abundant in the sediments of the cores 1015 and 1034 deposited during the interstadial MIS 3, with *B. subreticulata* being the dominant species. This species is associated to highly saline, and low oxygen waters (Gupta, 1994). Therefore, the ventilation of the Red Sea bottom waters was probably low during MIS 3, but higher than during MIS 2, particularly for the deepest waters. The benthic foraminifera assemblage of MIS 1 sediments corresponds

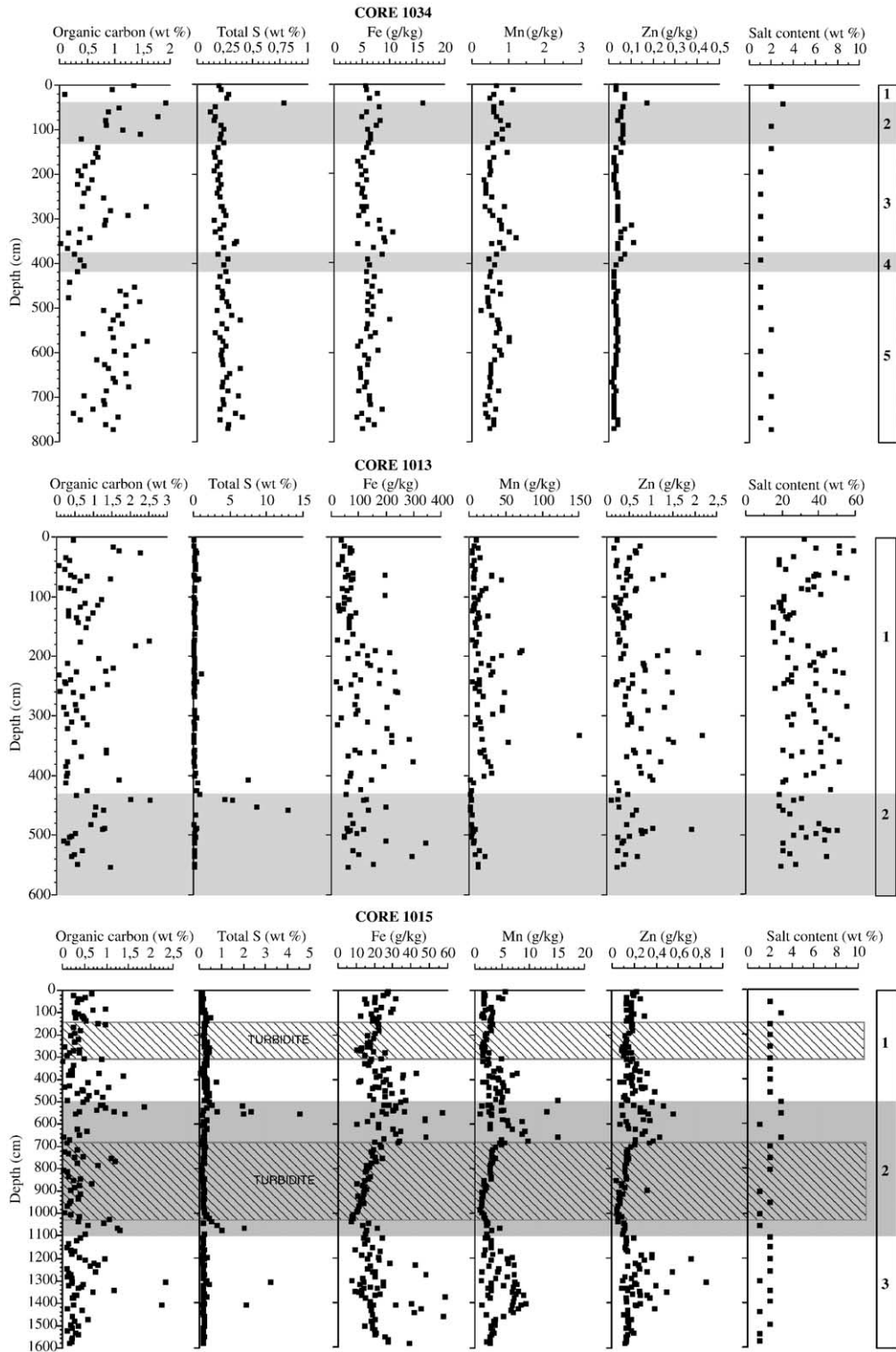


Fig. 5. Vertical profiles of particulate inorganic carbon, sulphur, metals (Fe, Mn, Zn) extracted with nitric acid, and salt content of dry samples.

Table 2  
Mean metal concentrations for individual MIS in cores 1034, 1013, and 1015

	1034			1013			1015		
	Fe	Mn	Zn	Fe	Mn	Zn	Fe	Mn	Zn
1000 m depth (g/kg)				Suakin Deep (g/kg)			Suakin plain (g/kg)		
MIS 1	6.4	0.72	0.05	99.6	19.4	0.63	21.9	2.9	0.17
MIS 2	7.5	0.73	0.07	117.3	5.7	0.53	28.2	5.2	0.24
MIS 3	6.0	0.62	0.04				22.3	4.5	0.29
MIS 4	6.7	0.56	0.04						
MIS 5	6.1	0.58	0.03						

Turbiditic layers of core 1015 have been extracted.

to present-day conditions, with well-oxygenated deep bottom waters (outside the hydrothermal brine pools).

#### 4.2. Effect of paleo-environment on the distribution of metals in the Red Sea sediments

Mn, Zn, and Fe concentrations vary according to sites and isotopic stage (Table 2). The core 1034 is relatively poor in particulate metal in comparison with the other studied cores. The sedimentation rate was smaller in the core 1034 than in the cores 1013 and 1015. Both depleted metal concentration and low sedimentation rate indicate that the flux of metals was much lower in the core 1034 than in sediments deposited deeper in the Red Sea axial zone. For example, we have calculated a mean flux of Mn of  $3.5 \text{ mg cm}^{-2} \text{ ky}^{-1}$ , using the mean values for concentration, sedimentation rate, and a porosity of 65%. The core 1034 is located outside the axial zone and it records probably the background metal flux of Red Sea sediment deposited at 1000 m depth, with a negligible influence of metal supplies from hydrothermal activity.

The variability of metal concentration was higher during the anoxic or dysoxic MIS 2 and 3 than during the stage 1 in the core 1015. The core was collected in the axial zone of the Red Sea at about 2000 m depth, but several kilometers apart from the hydrothermal Suakin basin. The sedimentation rate of the core 1015 did not vary significantly during MIS 1 and 2, when we extracted the turbiditic layers from the sediment column. Therefore, the fluctuations of metal concentrations represent the evolution of particulate metal fluxes to the sediment. Average concentrations reported in Table 2 indicate that the metal flux was lower in the core 1015 during MIS 1. For example, considering a porosity of 65% for the whole core, the mean flux of Mn was  $42 \text{ mg cm}^{-2} \text{ ky}^{-1}$  during MIS 1, and  $96 \text{ mg cm}^{-2} \text{ ky}^{-1}$  during MIS 2. More metalliferous particles were supplied to the Red Sea sediments at 2000 m

depth during the periods of low oxygenation, than during the Holocene.

The core 1013 collected within the Suakin brine pool shows the greatest metal concentrations. We calculated also the greatest metal fluxes. For example, the calculated mean flux of Mn is  $834 \text{ mg cm}^{-2} \text{ ky}^{-1}$  during MIS 1, where the sedimentation rate is available. The sediment of MIS 2 contains less Mn and Zn than the sediment of MIS 1. The jump of concentration is the most obvious for Mn, since the average concentration is  $19.4 \text{ g kg}^{-1}$  for MIS 1, and  $5.7 \text{ g kg}^{-1}$  for MIS 2 (Table 2). Such an increase of metal content from MIS 2 to 1, has already been observed in the metalliferous sediments of the Atlantis II Deep, where the increase of metal concentration corresponded to an increase of metal fluxes to the sediment (Anschutz and Blanc, 1995). Unfortunately, the core 1013 did not permit to calculate a sedimentation rate for the MIS 2 deposits. Therefore, it was not possible to evaluate the evolution of the metal fluxes between MIS 2 and MIS 1. Except for the sapropelic horizon, Pierret et al. (2000) observed, however, no significative changes in the lithology of the core 1013, which suggests that the difference in metal concentration is not a dilution effect with a major sediment component. Consequently, the great difference of metal concentrations suggests that, in contrast to the core 1015, the flux of metal to the sediment was lower during the LGM than during the Holocene in the Suakin Deep.

The flux of metals differs greatly from an environment to another. The flux of Mn in the core 1013 is more than one order of magnitude higher than the flux in the core 1015, which is one order of magnitude higher than in the core 1034. The very high metal fluxes in the core 1013 are related to the hydrothermal metal input in the Suakin Deep. The great difference in metal fluxes between the core 1015 and the core 1034 could be explained by diagenetic processes, such as metal remobilization in the core 1015 initiated by the turbidite deposition (Buckley and Cranston, 1988). However, such a process changes the vertical distribution of metals, but it should not affect significantly the average metal flux. The high metal fluxes in the core 1015 suggests that the Suakin plain was to some extent influenced by hydrothermal input. The evolution with time of particle metal fluxes could be linked to an evolution of the hydrothermal activity along the axial zone of the Red Sea. In that case, an increase or a decrease of metal input recorded in the axial zone sediment should be also recorded within the sediment of the brine-filled depressions. However, the decrease of hydrothermal metal input during MIS 1 in the core

1015 corresponds to a contemporaneous increase of metal flux in the adjacent Suakin Deep, but also in the Atlantis II Deep, which is the location of the most intensive hydrothermal activity in the Red Sea.

The spatio-temporal distribution of metals can be linked to the evolution of the oxygenation state of the Red Sea bottom waters, since Fe, Mn, and Zn have a mobility which changes with the redox state of the aqueous solution. Fe and Mn belong to a first group of transition metals, whose valency can vary as a function of prevailing redox potential (Calvert and Pedersen, 1993). They form highly insoluble oxide or hydroxide in oxic conditions. A second group, concern those elements which form highly insoluble sulphides in the presence of hydrogen sulphide ( $\text{H}_2\text{S}$ ) in anoxic conditions. Zn is included in this group. The solubility of reduced Fe also decreases sharply in the presence of sulphide. Fe and Zn precipitate as  $\text{ZnS}$  or  $\text{FeS}$ . Accumulation of Mn in sediments under oxic bottom waters is generally higher than under anoxic conditions, where Mn is soluble. The core 1015 presents an opposite situation, with a higher flux of Mn during MIS 2 than during MIS 1, which suggests that the variations of metal concentrations in the Red Sea axial zone were not linked to the redox state of waters alone, regardless of an additional source of metals, that is the hydrothermal activity.

In the Red Sea, metal enriched hydrothermal fluids originate from the leaching of the young oceanic basaltic crust and the Neogene sediments that formed during the opening of the Red Sea basin (Zierenberg and Shanks, 1988; Anschutz et al., 1995). The principal sediment formation consists of Miocene evaporites, which can reach several kilometers in thickness (Beydoun, 1989; Purser and Bosence, 1998). Therefore, the hydrothermal fluids are brines, which are trapped into topographic depressions, because their density are higher than the Red Sea bottom waters (Anschutz et al., 1998). Most of Fe and Zn precipitate quickly as sulphide minerals when reduced sulphide are supplied with the hydrothermal brine. Hydrothermal sulphide formation has been recognized in some sediment layers of the Atlantis II Deep. However, because the hydrothermal reduced sulphur concentrations are lower than the dissolved metal concentration in the hydrothermal fluids (Anschutz and Blanc, 1995), most of the metals cannot be trapped as sulphide, and precipitate at the brine–seawater interface, which consists of a redox barrier. The brine–seawater interface is a boundary between the well oxygenated seawater and the anoxic dissolved metal-rich brine. Profiles of particulate and dissolved metals in the brine of the Atlantis II deep

show that the Fe is quantitatively trapped as iron hydroxide at the interface, and that most of the Mn precipitates as oxihydroxide (Hartmann, 1985). Other metals, such as Zn, are adsorbed on the Mn and Fe precipitates. The profiles show that a small part of the dissolved Mn is able to escape the deep, because of the lower kinetics of Mn oxidation in the presence of oxygen than the oxidation of Fe (Stumm and Morgan, 1996). Therefore, in the present-day situation, and during all the Holocene, when the brine–seawater interface corresponded both to a pycnocline and to an oxicleine, most of the metals settled close to their source, at the bottom of the deeps.

The micropaleontological data of the core 1015 suggests that the oxicleine was located far above the present-day pycnocline of the Suakin Deep (2700 m) during MIS 2. The increase of volume of anoxic waters was not due to an extension of the brine pools following a tremendous increase of hydrothermal activity. Else, we should observe an increase of the salt content in the sediment of the bottom of the core 1015, which is not the case (Fig. 5). The formation of oxygen-free deep waters was due to climate and sea-level changes, which induced a lowering of the Red Sea deep water ventilation, as suggested by Fenton et al. (2000). Therefore, the brine–seawater interface was no more a redox barrier for the dissolved hydrothermal metals, which were able to diffuse over the large area covered by the anoxic waters. The oxidation–precipitation of the metals took place at the oxicleine, probably located between the depth of the core 1015 (2000 m) and the core 1034 (1000 m). Then, for a constant flux of hydrothermal metals, the sediment surface above which the metal oxide minerals precipitated was much wider during MIS 2 than during MIS 1. This scenario agrees with the metal distribution we observed, and is summarized in the Fig. 6. Since both the Atlantis II Deep and the Suakin Deep recorded lower fluxes of metals during MIS 2, we can suspect that the body of anoxic deep water was in connection with both hydrothermal systems. The connection is possible when the oxic–anoxic boundary is located at 1600 m depth, or above. A boundary at 1600 m depth covers a surface area of 5500  $\text{km}^2$ . For comparison, the surface area of the present-day anoxic brine of the Atlantis II Deep is 60  $\text{km}^2$ .

When the ventilation of a deep oceanic basin ceases, such as in the present-day Black Sea or Cariaco Basin, the environment becomes anoxic because of the oxygen consumption by respiration. Anaerobic degradation of organic matter occurs then, and bacterial sulphate reduction, and subsequent production of

dissolved sulphide, can take place. Dissolved sulphide was probably produced in the anoxic deep waters of the Red Sea during MIS 2. Then, the diffusion of the hydrothermal insoluble metals in the presence of sulphide, such as Fe and Zn, but not Mn, was most likely limited, and these metals precipitated as sulphide minerals at the brine–sulphidic waters interface. Such a situation could explain why the Mn showed higher concentration variations between MIS 1 and 2 in the cores 1015 and 1013, namely, higher mobility during the anoxic events. The proposed scenario also gives an explanation for the isotopic signature of the sulphide minerals in the Atlantis II Deep. The sulphide minerals of MIS 2 have an isotopic signature of sulphur typical of the bacterial seawater sulphate reduction, and not a basaltic hydrothermal signature such as the sulphides of MIS 1 (Shanks and Bischoff, 1980).

## 5. Conclusion

This study combines stratigraphic and geochemical data of three sedimentary cores collected in the axial zone of the Red Sea. The evolution of metal concentrations in the Red Sea sediments collected in the brine-filled deeps and in the axial zone outside the deeps, can be attributed to hydrothermal fluid discharge, but also to hydrological modification in the Red Sea. We have observed evidences of low oxygenation of Red Sea bottom waters during the last glacial period and the interstadial MIS 3. The oxygenation state of bottom waters influenced directly the geographical dissemination of the hydrothermal metals. The anoxia of the deep waters during MIS 2 as a consequence of Red Sea water stratification conducted to the formation of a redox boundary between 1000 and 2000 m depth, where the metals precipitated. This explains the observed increase

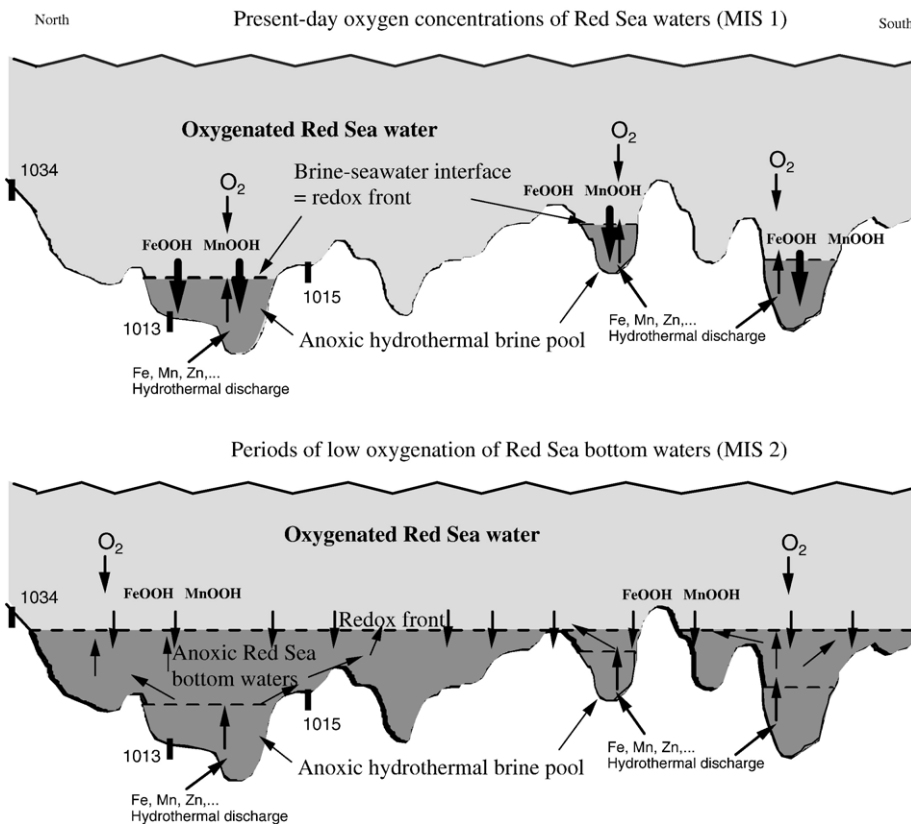


Fig. 6. Schematic cross-section along the axial zone of the Red Sea showing the position of the pycnocline (brine–seawater interface), and the position of the redox front, where metals are oxidized and precipitate. Top: Nowadays, and during the Holocene, the brine–seawater interface corresponds to the redox front where most of the metals supplied by hydrothermal fluids precipitate. The metalliferous sediments are confined into the hydrothermal deeps. Bottom: During MIS 2, bottom waters were anoxic and dissolved metals were able to diffuse outside the brine-filled deeps. They precipitated at the interface between oxic and anoxic seawater located between 1000 and 2000 m depth. When dissolved sulphide accumulated in the anoxic Red Sea bottom waters because of bacterial sulphate reduction, only Mn was able to diffuse. During the interstadial MIS 3, the situation was probably intermediate between the two situations.

of the particulate metal content during MIS 2 outside the brine pools. During interglacial periods, with well oxygenated bottom waters, the redox boundary was coincident with the brine–seawater interface, so that the metals precipitated only in the hydrothermal deeps. This study brings new elements to better understand the formation of metalliferous sediment in the Red Sea, and shows that the variations of particulate metal concentrations in the deeps during the last 30,000 years were not only related to fluctuations of the hydrothermal fluid discharge, but they were also related to the redox state of the Red Sea waters.

### Acknowledgements

The Ivory Coast Government is thanked for providing the student fellowship to A.C. We would also like to thank C. Pierre, E. Gonthier, H. Etcheber, G. Lavaux, K. Charlier, J. Schäfer, and F.J. Jorissen for beneficial discussions and technical support. We would like to express our gratitude to Jean-Pierre Tastet. The text was also significantly improved thanks to the comments of G. J. De Lange, D. Cronan, and an anonymous reviewer. The study was supported by the French program “Action Thématique Innovante” of the CNRS-INSU.

### References

- Ahmad, F., Sultan, S.A.R., 1987. On the heat balance terms in the central region of the Red Sea. *Deep-Sea Res.* 34, 1757–1760.
- Almogi-Labin, A., Luz, B., Duplessy, J.C., 1986. Quaternary paleo-oceanography, pteropod preservation and stable isotope record of the Red Sea. *Paleogeogr. Paleoclimatol. Paleocool.* 57, 195–211.
- Almogi-Labin, A., Hemleben, C., Meischner, D., Erlenkeuser, H., 1991. Paleoenvironmental events during the last 13,000 years in the central Red Sea as recorded by pteropoda. *Paleoceanography* 6, 83–98.
- Almogi-Labin, A., Hemleben, C., Meischner, D., 1998. Carbonate preservation and climatic changes in the central Red Sea during the last 380 Kyr as recorded by pteropods. *Mar. Micropaleontol.* 33, 87–107.
- Anschutz, P., Blanc, G., 1995. Chemical mass balances in metalliferous deposits from the Atlantis II Deep (Red Sea). *Geochim. Cosmochim. Acta* 59, 4205–4218.
- Anschutz, P., Blanc, G., Stille, P., 1995. Origin of fluids and the evolution of the Atlantis II Deep hydrothermal system, Red Sea: strontium isotopic study. *Geochim. Cosmochim. Acta* 59, 4799–4808.
- Anschutz, P., Turner, J.S., Blanc, G., 1998. The development of layering, the fluxes through double-diffusive interfaces, and the location of hydrothermal sources of brines in the Atlantis II Deep (Red Sea). *J. Geophys. Res.* 103, 27809–27819.
- Anschutz, P., Blanc, G., Chatin, F., Geiller, M., Pierret, M.C., 1999. Hydrographic change during 20 years in the brine-filled basins of the Red Sea. *Deep-Sea Res., Part 1, Oceanogr. Res. Pap.* 46, 1779–1792.
- Bäcker, H., Lange, K., Richter, M., 1975. Morphology of the Red Sea central graben between Subair Islands and Abul Kizan. *Geol. Jahrb.*, D 13, 79–123.
- Baumann, A., Richter, H., Schoell, M., 1973. Suakin Deep: brines and hydrothermal sediments in the deepest part of the Red Sea. *Geol. Rundsch.* 62, 684–697.
- Berggren, W.A., Boersma, A., 1969. Late Pleistocene and Holocene planktonic foraminifera from the Red Sea. In: Degens, E.T., Ross, A.D. (Eds.), *Hot Brines and Recent heavy Metal Deposits in the Red Sea*. Springer Verlag, Berlin, pp. 282–298.
- Beydoun, Z.R., 1989. The hydrocarbon prospects of the Red Sea–Gulf of Aden: a review. *J. Pet. Geol.* 12, 125–144.
- Blanc, G., Anschutz, P., 1995. New hydrographic situation in the Atlantis II Deep hydrothermal brine system. *Geology* 23, 543–546.
- Buckley, D.E., Cranston, R.E., 1988. Early diagenesis in deep sea turbidites: the imprint of paleo-oxidation zones. *Geochim. Cosmochim. Acta* 52, 2925–2939.
- Calvert, S.E., Pedersen, T.F., 1993. Geochemistry of recent oxic and anoxic marine sediments: implications for the geological record. *Mar. Geol.* 113, 67–88.
- Deuser, W.G., Ross, E.H., Waterman, L.S., 1976. Glacial and pluvial periods: their relationship revealed by Pleistocene sediments of the Red Sea and Gulf of Aden. *Science* 191, 1168–1170.
- Fairbanks, R.C., 1989. A 17,000 year glacio-eustatic sea level record: influence of glacial melting rates on the Younger Dryas event and deep ocean circulation. *Nature* 342, 637–642.
- Fenton, M., Geiselhart, S., Rohling, E.J., Hemleben, C., 2000. Aplanktonic zones in the Red Sea. *Mar. Micropaleontol.* 40, 277–294.
- Gupta, A.K., 1994. Holocene deep-sea benthic foraminifera and watermasses in the Indian Ocean and Red Sea. *J. Geol. Soc. India* 43, 691–703.
- Halicz, E., Reiss, Z., 1981. Paleocological relations of foraminifera in a desert enclosed sea—the Gulf of Aqaba. *Mar. Ecol.* 2, 15–34.
- Hartmann, M., 1985. Atlantis II deep geothermal brine system. Chemical processes between hydrothermal brines and Red Sea deep water. *Mar. Geol.* 64, 157–177.
- Hemleben, C., Meischner, D., Zahn, R., Almogi-Labin, A., Erlenkeuser, H., Hiller, B., 1996. Three hundred eighty thousand year long isotope and faunal records from the Red Sea. *Paleoceanography* 11, 147–156.
- Hofmann, P., Schwark, L., Brachert, T., Badaut, D., Rivière, M., Purser, B.H., 1998. Sedimentation, organic geochemistry and diagenesis of cores from the axial zone of the Red Sea: relationships to rift dynamics and climate. In: Purser, B.H., Bosence, D.W.J. (Eds.), *Sedimentation and Tectonics of Rift Basins: Red Sea–Gulf of Aden*. Chapman and Hall, pp. 479–504.
- Imbrie, J., Shackleton, N.J., Pisias, N.G., Morely, J.J., Prell, W.L., Martinson, D.G., Hays, J.D., McIntyre, A., Mix, A.C., 1984. The orbital theory of Pleistocene climate: support from a revised chronology of the marine  $d^{18}O$  record. In: Berger, A., et al. (Eds.), *Milankovitch and Climate*. D. Reidel, Hingham, Massachusetts, pp. 269–305.
- Ivanova, E.V., 1985. Late Quaternary biostratigraphy and paleotemperatures of the Red Sea and Gulf Aden based on planktonic foraminifera and pteropods. *Mar. Micropaleontol.* 9, 335–364.
- Ku, T.L., Thurber, D.L., Mathieu, G.G., 1969. Radio carbon chronology of Red Sea sediments. In: Degens, E.T., Ross, A.D. (Eds.), *Hot Brines and Recent Heavy Metal Deposits in the Red Sea*. Springer Verlag, Berlin, pp. 348–359.

- Locke, S.M., Thunell, R.C., 1987. Paleooceanographic record of the glacial–interglacial cycle in the Red Sea and Gulf of Aden. *Paleogeogr. Paleoclimatol. Paleoeconol.* 64, 163–187.
- Miller, A.R., Densmore, C.D., Degens, E.T., Hathaway, J.C., Manheim, F.T., McFarlin, P.F., Pocklington, H., Jokela, A., 1966. Hot brines and recent iron deposits in deeps of the Red Sea. *Geochim. Cosmochim. Acta* 42, 1103–1115.
- Milliman, J.D., Ross, D.A., Ku, T.L., 1969. Precipitation and lithification of deep sea carbonates in the Red Sea. *J. Sediment. Petrol.* 39, 724–736.
- Morcos, S.A., 1970. Physical and Chemical Oceanography of the Red Sea. *Oceanogr. Mar. Biol. Annu. Rev.* 8, 73–202.
- Pierret, M.C., Blanc, G., Clauer, N., 2000. Sur l'origine de la pyrite framboïdale dans les sédiments de la fosse Suakin (mer Rouge). *C. R. Acad. Sci. Paris* 330, 31–38.
- Pottorf, R.J., Barnes, H.L., 1983. Mineralogy, geochemistry, and ore genesis of hydrothermal sediments from Atlantis II Deep, Red Sea. *Econ. Geol. Monogr.* 5, 198–223.
- Purser, B., Bosence, D., 1998. Sedimentation and Tectonics in Rift Basins — Red Sea, Gulf of Aden. Chapman and Hall, London.
- Rohling, E.J., Fenton, M., Jorissen, F.J., Bertrand, P., Ganssen, G., Caulet, J.P., 1998. Magnitudes of sea-level lowstands of the past 500,000 years. *Nature* 394, 162–165.
- Scholten, J.C., Stoffers, P., Garbe-Schönberg, D., Moammar, M., 2000. Hydrothermal mineralization in the Red Sea. In: Cronan, D.S. (Ed.), *Handbook of Marine Mineral Deposits*. CRC Press LLC, pp. 369–395.
- Shanks III, W.C., Bischoff, J.L., 1980. Geochemistry, sulfur isotope composition and accumulation rates of the Red Sea geothermal deposits. *Econ. Geol.* 75, 445–449.
- Siddall, M., Rohling, E.J., Almogi-Labin, A., Hemleben, C., Meischner, D., Schmelzer, I., Smeed, D.A., 2003. Sea-level fluctuations during the last glacial cycle. *Nature* 423, 853–858.
- Stumm, W., Morgan, J.J., 1996. *Aquatic Chemistry*, 3rd edition. J. Wiley and Sons, New York.
- Thunell, R.C., Locke, S.M., Williams, D.F., 1988. Glacio-eustatic sea-level control on Red Sea salinity. *Nature* 334, 601–604.
- Werner, F., Lange, K., 1975. A bathymetric survey of the sill area between the Red Sea and the Gulf of Aden. *Geol. Jahrb.* 13, 125–130.
- Zierenberg, R.A., Shanks III, W.C., 1988. Isotopic studies of epigenetic features in metalliferous sediments, Atlantis II deep, Red Sea. *Can. Mineral.* 26, 737–753.